ACS APPLIED MATERIALS & INTERFACES



Article

# Triphenylamine based Metal-Organic Frameworks as Cathode Materials in Lithium Ion Batteries with Coexistence of Redox Active sites, High working voltage, and High rate stability

Zhe Peng, Xiaohui Yi, Zi Xuan Liu, Jie Shang, and Deyu Wang

*ACS Appl. Mater. Interfaces*, **Just Accepted Manuscript** • DOI: 10.1021/acsami.6b03418 • Publication Date (Web): 26 May 2016



## Just Accepted



ACS Publications

ACS Applied Materials & Interfaces is published by the American Chemical Society.
1155 Sixteenth Street N.W., Washington, DC 20036

# Triphenylamine based Metal-Organic Frameworks as Cathode Materials in Lithium Ion Batteries with Coexistence of Redox Active sites, High working voltage, and High rate stability

*Zhe Peng*[a]*, *Xiaohui Yi*[bc]*, *Zixuan Liu*[a], *Jie Shang*[bc], *Deyu Wang*[a]

a. Institute of New Energy Technology, Ningbo Institute of Materials Technology and Engineering, Chinese Academy of Sciences, Ningbo 315201, China.

b. Key Laboratory of Magnetic Materials and Devices, Ningbo Institute of Materials Technology and Engineering, Chinese Academy of Sciences, Ningbo 315201, China.

c. Zhejiang Province Key Laboratory of Magnetic Materials and Application Technology, Ningbo Institute of Materials Technology and Engineering, Chinese Academy of Sciences, Ningbo 315201, China.

Keywords: Metal-organic framework, Lithium-ion battery, Redox activity, Coulombic efficiency, Capability rate.

**Abstract:** Through rational organization of two redox active building block, a triphenylamine based Metal-Organic Framework (MOF) material, Cu-TCA ($H_3TCA$ = tricarboxytriphenyl amine), was synthesized and applied as a cathode active material for the first time in lithium batteries. The Cu-TCA exhibited redox activity both in the metal clusters ($Cu^+/Cu^{2+}$) and organic ligand radicals ($N/N^+$) with separated voltage plateaus and a high working potential vs. $Li/Li^+$ up to 4.3 V, comparable with the current commercial $LiCoO_2$ cathode materials. The electrochemical behaviors of this MOF electrode material at different states of charge were carefully studied by cyclic voltammetry, X-ray photoelectron spectroscopy and photoluminescence techniques. Long cycling stability of this MOF was achieved with an average Coulombic efficiency of 96.5% for 200 cycles at 2 C rate. Discussing the electrochemical performances on the basis of capacity contributions from the metal clusters ($Cu^+/Cu^{2+}$) and organic ligands ($N/N^+$) conducts to propose an alternative mechanism of capacity loss for the MOF materials used in lithium batteries. This improved understanding will shed light on the designing principle of MOF-based cathode materials for their practical application in battery sciences.

## 1. Introduction

In the past decade, the market of Li-ion battery (LIB) exhibited a phenomenal growth owing to its high energy density and large output current.[1] The conventionally used cathode active materials in the LIBs are layered metal oxides or metal salts, such as $LiCoO_2$ or $LiFePO_4$.[2] Nevertheless, the formation of insulating metal oxide layers at their interface causes high potential barrier for the redox reactions and limited recharge rate, and the lack of efficient $Li^+$ ions diffusion paths through the bulk phase of the active material lead to incomplete lithiation/delithiation.[2-3]

Metal-organic frameworks (MOFs), a class of hybrid materials based on networked structure consisting of metal ions or clusters that are connected by electron-donating organic ‘‘linker’’ groups, has been highlighted as a family of crystalline solids due to their highly porous structure, exceptional structural tunability and practical production cost compared to conventional inorganic materials. The MOF materials are widely applied in gas storage and selection,[4-5] molecule recognition[6] and enantioselective catalysis,[7] but only a few studies to date have reported their application in LIBs.[8-10] Compared to conventional inorganic cathode materials, the MOFs are expected to undergo improved electrochemical properties such as better electrolyte accessibility and higher ion-diffusion rate, due to their large ion diffusion tunnels provided by the porous structures. The conventionally used MOF materials possessed redox activity only on their metal clusters with redox-innocent ligands.[8-9] Though the redox-active organic ligands have been developed for LIBs recently,[11-14] there was till 2014 the first study that reported the MOF material with coexistence of redox activities as cathode material in LIBs,[10] by combining the metal clusters with redox-active organic ligands. This work indicated that introducing both redox active organic ligands and metal clusters into porous MOF structure was an efficient approach to

form high capacity cathode materials in Li-ion batteries.[10] However, low working voltage (below 4 V) and relatively short cycling life remain problematic for the practical application of this kind of MOFs in LIBs, and better understanding of capacity loss in the MOFs materials is urgently demanded.

Among the vast variety of MOFs materials, Cu-TCA ($H_3TCA$ = tricarboxytriphenyl amine) has attracted our attention due to its porous structure (the reported theoretical radii of the pore was 1 nm and the free volume was 79.7% for fully desolvated Cu-TCA)[15] and abundant redox active constituents, which are the $Cu^{2+}$ ions located at the metal cluster sites and N atoms bonded with three neighbor benzene rings in tripenylanmine of the organic ligand (Figure 1a).[15-16] It was first employed as a selectively sensing material due to its variable fluorescent sensibility while the redox change between $Cu^{+2}$ and $Cu^{+}$ took place.[15] Further, it has been reported that the redox active transition between neutral and cationic forms of the N atoms in the triphenylamine-based ligand exhibited reliably thermal stablility.[16] Herein we applied the Cu-TCA as cathode material in LIB for the first time. Thanks to the abundant redox active constituents and very stable organic ligands, the theoretical capacity of the Cu-TCA is 145 mAh $g^{-1}$, comparable with the commercial materials (i.e., $LiFePO_4$, 170 mAh $g^{-1}$), and the working voltage could rise up to 4.3 V, which is comparable with the current commercial $LiCoO_2$ cathode materials. Interesting electrochemical behaviors with separated redox plateaus have been observed and identified through cyclic voltammetry, X-ray photoelectron spectroscopy and photoluminescence studies. Long cycling stability over 200 cycles at 2 C rate was achieved by this MOF with an average Coulombic efficiency of 96.5%. This suggested that the porous spaces of the Cu-TCA may allow high recharge rate without degrading the capacity retention. More important, we gave an interpretation for the electrochemical performances from each redox couple and proposed an

alternative capacity loss mechanism for MOF-based cathode materials. The latter, to best knowledge, has not yet been reported elsewhere and will shed light on the designing principle of MOF-based cathode materials for their practical application in battery sciences.

## 2. Experimental section

### 2.1 Cu-TCA synthesis

All reagents were of analytical grade and used as received. 0.1 mmol $Cu(NO_3)_2$ was dissolved in a 1:1 volume mixture of 10 ml N,N-Dimethylformamide, DMF and 10 ml $CH_3OH$ solution. 0.2 mmol NaOH was dissolved in 10 ml $CH_3OH$ solution and added into the $Cu(NO_3)_2$-DMF-$CH_3OH$ solution to form $Cu^{2+}$ hydroxide suspension. Then a solution of 0.1 mmol $H_3TCA$ (Tricarboxytriphenyl amine) in 10 ml DMF was added in the suspension and stirred till deep green precipitation was generated, this solution was finally filtrated to obtain the Cu-TCA powders. The obtained powders were directly used without any normal activation method such as thermal vacuum evaporation, since the latter induced a collapse of the porous MOF structure upon the Cu-TCA powders leading to a drastic capacity loss in the battery. Nitrogen gas adsorption and desorption measurement was carried out on an ASAP2020 analyzer from Micromeritics, Inc. The activation of MOF was performed at 120℃ under vacuum for 8 hours before measurement. The adsorption and desorption was performed at 293 K.

### 2.2 Electrode preparation

The prepared Cu-TCA, Super-P and Polyvinylidene fluoride, PVdF were mixed at a weight ratio of 8:1:1 in N-Methyl-2-pyrrolidone, NMP (Aladdin Industrial Inc.) till fully homogeneous slurry was obtained. Thermal gravimetric analysis (TGA) indicates that ~45% of the as-prepared MOF weight was contributed to the solvent molecules (12% for $CH_3OH$ and 33% for dimethylformamide, DMF, Figure S1b). The effective quantity of the Cu-TCA powder was

estimated as 55% of the weight used in the slurry for electrode preparation. The slurry was cast onto Al foils. After vacuum drying at 120℃ for 12h, the electrodes were obtained and transferred in argon-filled glove box (MBRAUN, $H_2O \leq 0.1$ ppm, $O_2 \leq 0.1$ ppm) for further cell assembly. The active material loading of as-prepared MOF electrodes was ~0.5 mg $cm^{-2}$.

**2.3 Electrochemistry**

Cyclic voltammetry (CV) and electrochemical impedance spectroscopy (EIS) tests were carried out using an electrochemical workstation 1470E equipped with a frequency response analyzer, FRA 1455A from Solartron. The CV measurements were performed between 1.4 and 4.3 V vs $Li/Li^+$ at a scanning rate of 1 mV $s^{-1}$. The EIS measurements were performed on the frequency range between $10^{-1}$ and $10^5$ Hz with a voltage perturbation of 5 mV. To record the EIS spectra at different electrochemical states of the Cu-TCA electrode, the CV scanning were coupled with EIS to sweep the electrode to desired potentials, than followed by the EIS measurements in holding the achieved potentials.

Cycling tests were performed using a battery testing system (LandCT2001 from LAND electronics Co., Ltd.). Cu-TCA electrodes were used as working electrodes. Li foils were used as counter electrodes. Coin cells CR2032 were used for cell assembly, with Celgard separator film (diameter: 18 mm; thickness: 20 μm) in which an electrolyte amount of 70 μL was deposed. The electrolytes consisted of a commercial electrolyte (1M $LiPF_6$ in 1:1 ethylene carbonate, EC and dimethyl carbonate, DMC, Guotai-Huarong New Chemical Materials Co., Ltd.). Two capacity rates (0.5 and 2 C) were tested within a voltage window of 1.4 and 4.3 V vs $Li/Li^+$ for 200 charge-discharge cycles.

**2.4 Electrode characterizations**

To characterize the cycled Cu-TCA electrodes, the cells were carefully disassembled in glove box, rinsed with pure DMC in order to eliminate residual trace of solvents and salts, and then stored in glove box for further characterization.

The microscopy analysis of the electrode surface morphology was performed using scanning electron microscopy (SEM, FEI, QUANTA 250 FEG) and transmission electron microscopy (TEM, FEI, Tecnai F20, 200 kV). The crystalline phase of the prepared samples was characterized by X-ray diffraction (XRD) with a Bruker D8 advanced diffractometer using CuKα ($\lambda$ = 1.5406 Å) radiation (Bruker axs, D8 Advance) between 5° and 45° in 0.02° step per second. Surface analysis was conducted with a PHI 3056 X-ray photoelectron spectrometer (XPS), which was excited by an MgKα radiation source at a constant power of 100 W (15 kV and 6.67 mA). The spectrum fitting was performed with the CasaXPS software. Photoluminescence of the electrode was studied by a confocal microscopy consisted of a laser source ($\lambda$=325 nm) and an Andor SR-303i spectrometer. All the sample preparations were performed under air-condition.

## 3. Result and Discussion

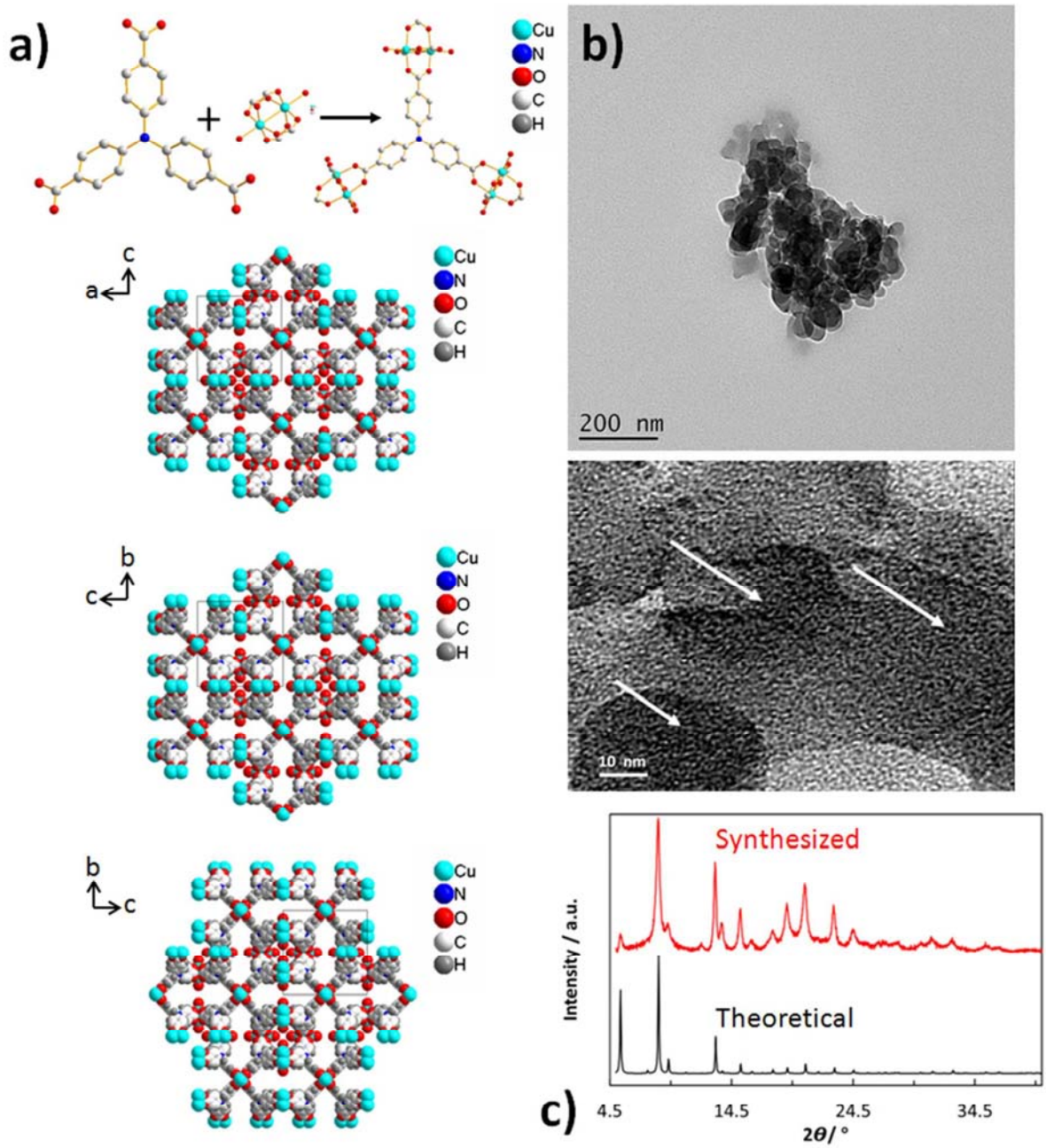


**Figure 1.** Schematic representation of the Cu-TCA structure (a); TEM images of the prepared Cu-TCA powders (b); XRD spectrum of the synthesized Cu-TCA and its theoretical spectrum (c); XRD patterns at small angles of Cu-TCA powders and electrode.

The Cu-TCA powders were synthesized through a simple solution-mixture method in ambient condition. The transmission electron microscopy (TEM) images of the synthesized Cu-TCA powders confirmed the porous structures of this material, as shown in Figure 1b. The X-ray diffraction (XRD) spectrum of the synthesized sample was similar to the theoretical one (generated from crystallographic information file of the Cambridge Crystallographic Data Centre (CCDC) number: 841879, Figure 1c).[15] The Brunauer−Emmett−Teller (BET) fitness suggested a surface area of as-prepared Cu-TCA powders after activation is ~180 $m^2$ $g^{-1}$ (Figure S1a). This value can be further improved by optimizing the activation method to prevent the partial collapse of the porous structure.

The cyclic voltammograms of Cu-TCA were recorded using a Li foil as counter electrode, as shown in Figure 2a. Two large reductive (4.3-3.4 V and 2.1-1.4 V) and oxidative (2.8-3.7 V and 3.7-4.3 V) waves are observed in the first cyclic voltammetry (CV) cycle of Cu-TCA (Figure 2a), respectively. To assess the origin of these redox areas, CV curves of the electrodes with pure TCA and Cu-TCA were taken in comparison. The reductive (2.1-1.4 V) and oxidative (2.8-3.7 V) waves were only observable in the CV curve of Cu-TCA, suggesting that they correspond to the redox reaction of $Cu^{+}/Cu^{2+}$. The reductive and oxidative waves located at 4.3-3.4 V and 3.7-4.3 V could originate from the organic ligand of triphenylamine in which the N atoms should act as the redox sites ($N/N^{+}$). One should be noted that an overlap in oxidative peaks may exist between the $Cu^{+}/Cu^{2+}$ and $N/N^{+}$ since the redox peaks are significant in the range of 3.5-4.3 V, however, as we will show later, even an overlap exists in oxidation, it does not affect the distinction in capacity contribution from the $Cu^{+}/Cu^{2+}$ and $N/N^{+}$ couples, since we compared the discharge curves where the reductive potentials between these redox couples could be clearly distinguished. The origin of these two redox areas was further investigated by X-ray photoelectron

spectrometer (XPS), *vide infra*. The CV curve of a bare electrode (only containing the Al foil) proves that the above-mentioned redox areas originate from the active sites of the MOF structure.

The charge-discharge test of the coin cell (Cu-TCA as working electrode and Li foil as counter electrode) was conducted at 0.5 C rate. After a pre-discharge, two separated plateaus were observed for the 1$^{st}$ charge (2.9-3.5 V and 3.8-4.3 V) and discharge (4.3-3.9 V and 2-1.8 V) (Figure 2b), which are consistent with the results of CV measurements (2.9-3.5 V in charge and 2-1.8 V in discharge for $Cu^{+}/Cu^{2+}$) and (3.8-4.3 V in charge and 4.3-3.9 V in discharge for $N/N^{+}$). The 1$^{st}$ charge capacity was 139.1 mAh $g^{-1}$ at the cut-off potential of 4.3 V, close to the theoretical capacity of the Cu-TCA (145 mAh $g^{-1}$). It should be noted that the pre-discharge (Figure 2b) served as an electrochemical activation of the Cu-TCA electrode (insertion of $Li^{+}$ ions into the Cu-TCA material). However, there was a gap in capacity between the pre-discharge and the 1$^{st}$ discharge (Figure 2b), which seems to be related to a self-adsorption of $Li^{+}$ ions by the MOF structure during cell assembly. Similar behaviors have been observed in the related works by Yoshikawa et al.[13] and Wang et al.[14] in which the redox active polymers could be directly charged after the cell assembly, where the charge capacity could only originated from the self-adsorbed $Li^{+}$ ions.

To further confirm the electrochemical observations, four states on the 1$^{st}$ charge and discharge process (Figure 2b), i.e. the charged states at 3.45 V (state I) and the cut-off potential of 4.3 V (state II), the discharged states at 2 V (state III) and the cut-off potential of 1.4 V (state III), are probed by XPS. As shown in Figure 2c, at initial state, no Li was found at a probed depth of several nm (< 10nm) from the material surface, shown by the Li 1s spectra. The electrode was then pre-discharged (lithiation) to 1.4 V, followed by the 1$^{st}$ charge to 3.45 V (state I) where one part of previously inserted Li-ions could still be probed by XPS. At fully charged state (state II),

much weaker signal of Li was observed, indicating a full delithiation. The Li 1s signal appeared again following the 1st discharge (state III and IV).

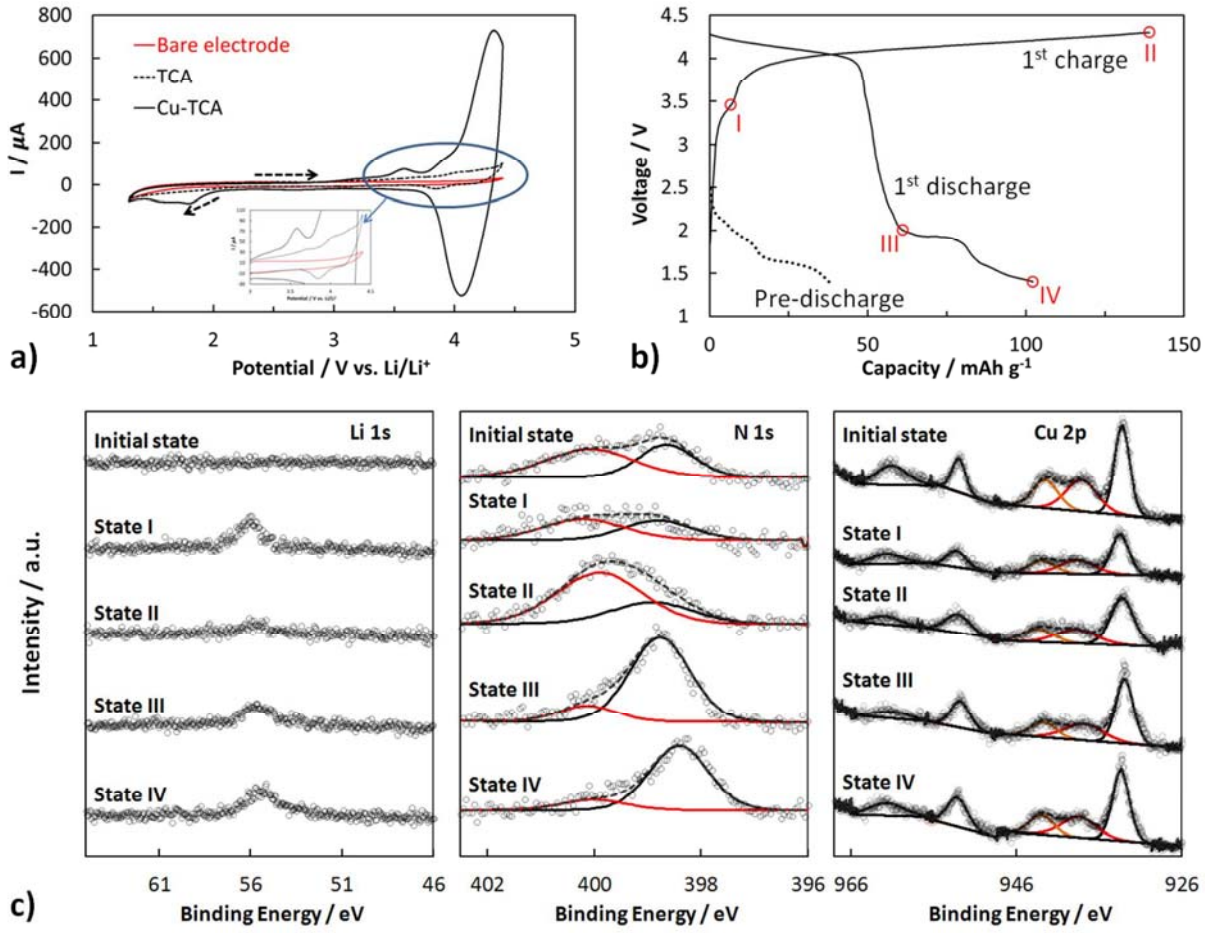


**Figure 2.** CV curves of the bare electrode, electrode with pure TCA and Cu-TCA (a); Voltage profiles of the 1st charge and discharge of the Cu-TCA electrode, the pre-discharge served as an electrochemical activation of the Cu-TCA electrode (b); XPS spectra of Li 1s, N 1s and Cu 2p of the Cu-TCA (c), at different electrochemical states as indicated in (b).

The oxidation and reduction of the N atoms in triphenylamine are observed in the N 1s spectra. In the initial state, two peaks located at 398.6 and 400.2 ev are deconvoluted, indicating the existence of both neutral and oxidized N species due to the partial oxidation in air.[17] In the charging process, no difference was found in N 1s spectra between the initial state and the state

charged to 3.45 V (state I), indicating that the oxidation of the N took place above the charge plateau of 3.45 V. Through one electron oxidation of N atoms in the charging process, the band at 398.6 eV attributed to the neutral state of N atoms is decreased and shifted to higher energy at 400.2 eV, which attributed to the oxidation of N atoms in fully charged state of 4.3 V (state II). Thus, the shift of N 1s spectra is consistent with the oxidative area observed in CV (3.4-4.3 V). Inversely, the overlap shifted to a lower energy with increased band at 398.6 eV up to the state III, and no more difference was found between states III and IV, indicating that the reduction process of the N atoms was completed above the discharge plateau of (2–1.8 V), and the latter should be related to the Cu reduction.

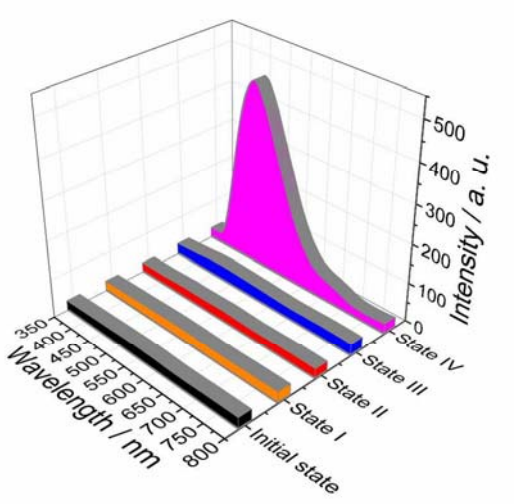


**Figure 3.** Luminescent emission spectra of the Cu-TCA electrodes at different electrochemical states as indicated in Figure 2b.

The distinction between $Cu^{+}$ and $Cu^{2+}$ is still an open question for the experts in the XPS field, and no decisive argument is reported to date even using complementary technic such as Auger electron spectroscopy, AES.[18] As shown in Figure 2c, we can only confirm the ionic state of Cu with the Cu 2p shake-up satellite lines at 938.2, 942.3, and 962.2 eV, and no evident difference can be caught out among different states. In this case, luminescent emission spectroscopy was

used to evidence the valence states of the Cu metal clusters. Different luminescent behaviors of the Cu-TCA electrode were observed at the aforementioned electrochemical states (Figure 3). At the initial state and states I, II and III, the luminescence of the TCA ligand was quenched when excited upon UV irradiation, the latter should be due to the existence of paramagnetic species $Cu^{2+}$. However, when the discharging process was shifted to the IV state, obvious fluorescence from 400 to 600 nm was observed, suggesting that at the IV state, the paramagnetic species $Cu^{2+}$ should be reduced into the diamagnetic species $Cu^{+}$ which will not quench the fluorescence of the TCA ligand. The observation in luminescent behavior is consistent with the results reported in the literature[15], and confirms the valence states of Cu ions from the observed electrochemical behaviors.

The $Li^{+}$ ions transfer kinetics in the Cu-TCA electrodes was further investigated by electrochemical impedance spectroscopy (EIS). Figure 4a shows the Nyquist plots for the different electrochemical states indicated in Figure 2b. With the frequency range of $10^{-1}$ - $10^{5}$ Hz, each of the curves has a depressed semicircle in the high-to-medium frequency and an oblique line in the low-frequency. The high frequency intercept impedance is attributed to the resistance of $Li^{+}$ ions transfer through the electrolyte ($R_{\Omega}$). The depressed semicircle in the medium frequency region is related to the resistance of charge movement ($R_{ct}$) at the electrolyte/electrode interface. The inclined line at low frequency associated with the Warburg impedance ($Z_{w}$), representing the $Li^{+}$ ions diffusion inside the bulk phase of the Cu-TCA materials.

Interestingly, the EIS spectra highly depended on the electrochemical states of Cu and N in the Cu-TCA ($Cu^{+}$ and N for the states pre-charged and IV; $Cu^{2+}$ and N for the states I and III; $Cu^{2+}$ and $N^{+}$ for the state II, Figure 4a and b). The bulk resistance $R_{\Omega}$ has been found similar ~ 3.6 **Ω** $cm^{2}$ through all the electrochemical states. The lowest $R_{ct}$ ~ 700 **Ω** $cm^{2}$ and $-\boldsymbol{\theta}$ (Z'/Z'') ~ 16°

(the incline of the Warburg impedance, $Z_w$) were found at the fully charged state ($Cu^{2+}$ and $N^+$), indicating that the dominant kinetics at this state was the charge-transfer at the electrolyte/electrode interfaces. Between states ($Cu^+$, N) and ($Cu^{2+}$, N), it seems that the diffusive impedance (the Warburg impedance, $Z_w$) was higher at the state ($Cu^+$, N) with its higher $-\boldsymbol{\theta}$ (Z'/Z'') ~ 76° than this of 67° at the state ($Cu^{2+}$, N), as shown in the Figure 4b. This observation suggests that part of the $Li^+$ ions was restricted at the state ($Cu^+$, N).

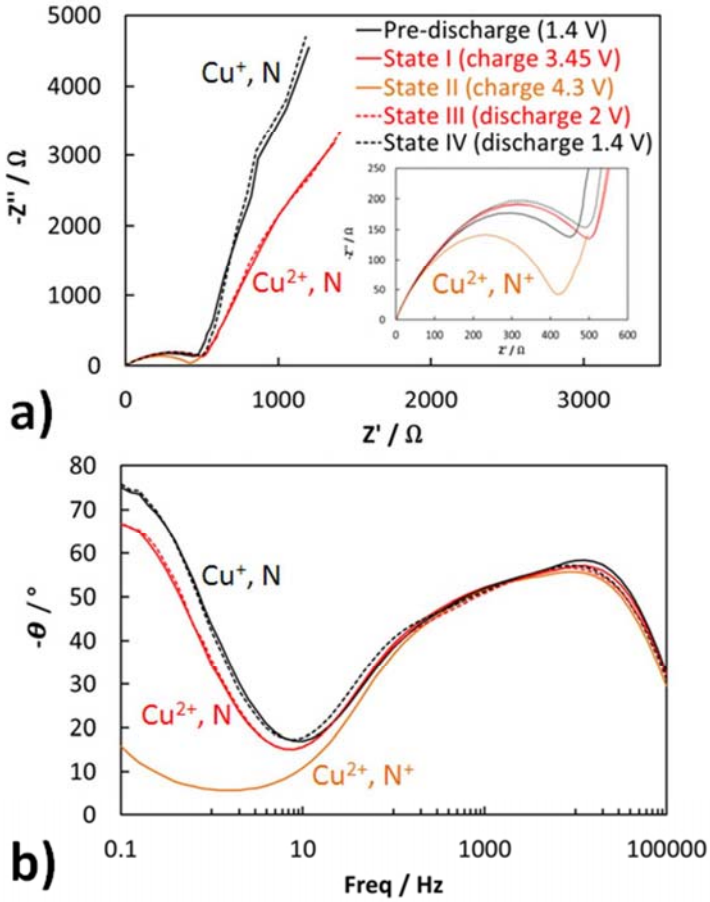


**Figure 4.** EIS spectra of the Cu-TCA electrode at different electrochemical states as indicated in Figure 2b (a); $-\boldsymbol{\theta}$ (Z'/Z'') vs. Freq plots of the EIS spectra (b).

Before the long cycling test in the coin cell, 50 successive CV cycles were performed to monitor the loss of redox activity in the MOF. As shown in the Figure 5a, the redox waves of

$Cu^{+}/Cu^{2+}$ couple (2.1-1.4 V and 2.8-3.7 V) disappeared at the $10^{th}$ cycle, while the waves of $N/N^{+}$ couples (4.3-3.4 V and 3.7-4.3 V) were not affected. This suggests that the loss of redox activity firstly took place on the Cu metal clusters, followed by the loss of redox activity of the radical N bonded with the 3 benzenes (see $10^{th}$, $25^{th}$ and $50^{th}$ of the CV cycling, Figure 5a).

Long cycling test in the coin cell was performed with a charge-discharge rate of 0.5 C. As shown in Figure 5b and c, the capacity fading was considerable, for example, for the $1^{st}$, $100^{th}$ and $200^{th}$ cycles, the discharge capacities were 102.2 mAh $g^{-1}$, 54.5 mAh $g^{-1}$ and 39.9 mAh $g^{-1}$, respectively. This order of capacity loss seems to be related to the loss of redox activity on the Cu ions, i.e. the $Cu^{+}/Cu^{2+}$ redox sites supplied 40% of the capacities at the $1^{st}$ cycle and 33% at the $100^{th}$ cycle, while at the $200^{th}$ cycle, the capacity contribution supplied by the $Cu^{+}/Cu^{2+}$ was decreased to only 22% (Table 1).

A more detailed mechanism of capacity loss in the Cu-TCA could be proposed. The capacity retention of only ~63% during the first 10 cycles could be attributed to the loss of the $Cu^{+}/Cu^{2+}$ redox sites. According to the recent research on the MOF-based Li solid electrolyte, the electronegativity of the oxygen atoms on the carboxyl group of an organic ligand is high and dominant.[19] In our case, probably, the electronegativity of the carboxylic O atoms surrounding the Cu ions becomes even more dominant while the $Cu^{2+}$ ions were reduced to $Cu^{+}$, which may make these O atoms strongly interact with $Li^{+}$ ions, causing the restriction of the $Li^{+}$ ions and uncompleted redox reactions on the Cu ions. This argument is in agreement with the observation in EIS results. Moreover, these interactions may weaken the Cu-O bonding and release the Cu ions from the MOF structures, which result in the instability of the structures and the capacity fading. Besides, further capacity loss could also be due to the inhomogeneity of crystal size and distribution in the cathodes, which may induce the incomplete exposure of the MOF internal

surface to the electrolyte, leading to a partial redox activity of $Cu^{+}/Cu^{2+}$ and $N/N^{+}$ couples (4.3-3.4 V and 3.7-4.3 V) from the $10^{th}$ to $200^{th}$ cycles. It is noted that the $Li^{+}$ ions intercalation has an effect on the framework structure of the Cu-TCA electrode before/after cycling, which could not be observed by SEM (Figure S2) but by XRD (Figure 5d). Consistently, little XPS signal of Cu 2p was detectable at a probed depth ~ several nm (< 10 nm) from the disassembled electrode since they were partially released from the MOF structure, while the spectrum of N 1s was still marked (Figure S3).

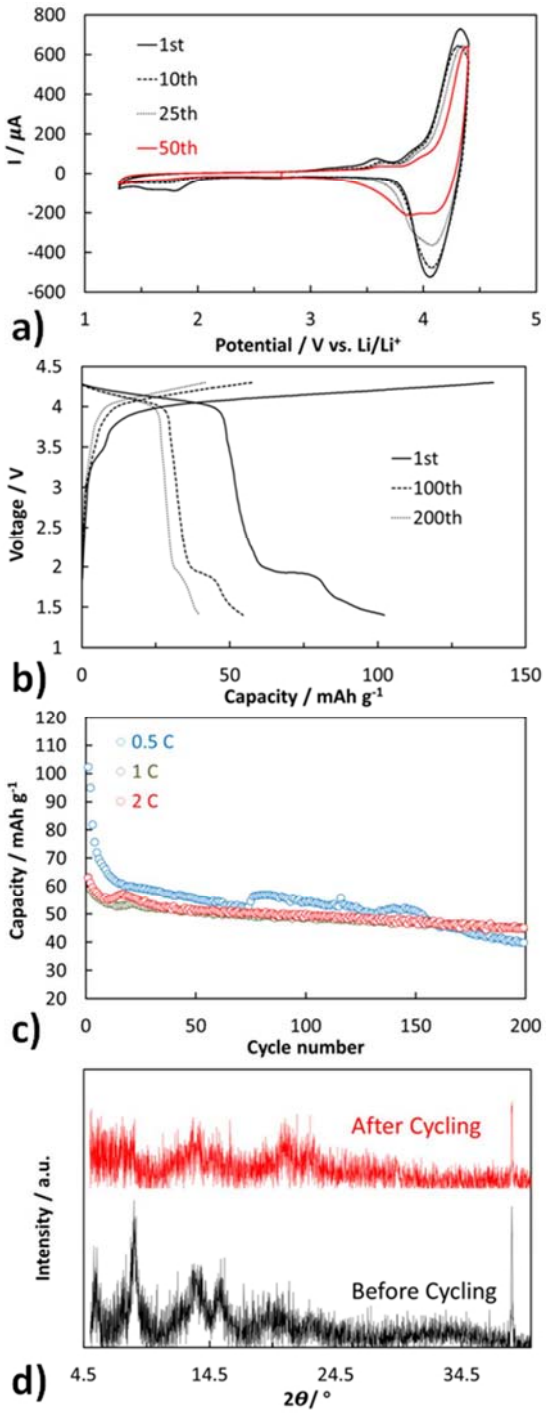


**Figure 5.** CV curves of the Cu-TCA for 50 cycles (a); Voltage profiles of the 1st, 100th and 200th cycles of the Cu-TCA electrode cycling at 0.5 C rate (b); Capacity evolutions of the Cu-TCA

electrodes for 200 cycles at 0.5, 1 and 2 C rates (c); XRD spectra of the Cu-TCA electrode before and after cycling (d).

The rate capability was also tested in the coin cell system, as shown in Figure 5c. Similar performances have been obtained at 1 C and 2 C rates, with capacity retentions at the 200$^{th}$ cycle of 70.9% for 1 C (discharge capacities of 63.2 and 44.8 mAh $g^{-1}$ for the 1$^{st}$ and 200$^{th}$ cycles) and 71.5% for 2 C (discharge capacities of 63.1 and 45.1 mAh $g^{-1}$ for the 1$^{st}$ and 200$^{th}$ cycles). The average Coulombic efficiencies were 97.2% and 96.5% for 1 C and 2 C, respectively. In the conventional cathode materials, the performances at high capability rates are generally poorer than these at low capability rates, while in the Cu-TCA, its performances could be maintained between 1 C and 2 C. The latter suggested that the porous structure of the Cu-TCA could be advantageous to sustain its rate capability without degrading the capacity retention.

It should be noted that at 0.5 C, the capacity retention was only 39% at the 200$^{th}$ cycle (discharge capacities of 102.2 and 39.9 mAh $g^{-1}$ for the 1$^{st}$ and 200$^{th}$ cycles), much lower than 70.9% at 1 C and 71.5% at 2 C. The charge-discharge profiles (Figure S4) also shown that the contribution from the metal clusters and organic ligands evolved less at 2 C than in case of 0.5 C (Table 1). The cell polarization should be considered and may account for these observations, by comparing the voltages in the two rates at a given capacity. For example, during the first charge, at the charge capacity of 75.8 mAh $g^{-1}$, the cut-off potential of 4.3 V was achieved at 2 C rate (Figure S4), while the voltage at this stage was only 4.1 V at 0.5 C (Figure 5b). Since the cell cycling at 2 C rate reached more easily the cut-off potential leading to incomplete lithiation/delithiation, this incomplete lithiation/delithiation may lead to only partial participation of the active sites to redox reactions, resulting probably in less degradation of the MOF structure and slower loss of active redox sites than in case of 0.5 C, thus affording better cycling stability.

To achieve a better understanding on this performance dependency on the rate capability, a further work to monitor the valence change of Cu and N in the Cu-TCA electrodes using *in situ* K-edge X-ray absorption near edge structure (XANES) analysis will be investigated by our group, with the aim of revealing the dynamics of the redox active sites ($Cu^{+}/Cu^{2+}$ and $N/N^{+}$) during the cycling of the Cu-TCA electrodes.

**Table 1. Rate capability tests data**

| | 1st cycle | | | 100th cycle | | | 200th cycle | | |
|---|---|---|---|---|---|---|---|---|---|
| Rate | Discharge capacity (mAh $g^{-1}$) | From $Cu^{+}/Cu^{2+}$ | From $N/N^{+}$ | Discharge capacity (mAh $g^{-1}$) | From $Cu^{+}/Cu^{2+}$ | From $N/N^{+}$ | Discharge capacity (mAh $g^{-1}$) | From $Cu^{+}/Cu^{2+}$ | From $N/N^{+}$ |
| 0.5 C | 102.2 | 40% | 60% | 54.5 | 33% | 67% | 39.9 | 22% | 78% |
| 2 C | 63.1 | 35% | 65% | 50 | 34% | 66% | 45.1 | 27% | 73% |

To improve the cyclic stability of the Cu-TCA electrodes, we used hexamethylene diisocyanate (HDI), an electrolyte additive that has been used to improve the performance of high-voltage cathode materials such as $LiNi_{1/3}Co_{1/3}Mn_{1/3}O_2$ by forming a protective layer at their surface through the coordination effect.[20-21] With a concentration of 1 mM HDI in an electrolyte of 1 M $LiPF_6$ in propylene carbonate (PC) : dimethyl carbonate (DMC) (1:1 in volume), the performances of the Cu-TCA were improved (Figure 6). Compared to the initial system, the discharge capacity at 2 C rate was raised from 63.1 to 75.3 mAh $g^{-1}$ for the 1st cycle, from 45.1 to 56.1 mAh $g^{-1}$ for the 200th cycle. The capacity retention at the 200th cycle was 74.5% in the optimized electrolyte, slightly higher than 71.5% in the initial system. As comparison, the capacity retentions of the $LiNi_{1/3}Co_{1/3}Mn_{1/3}O_2$ electrodes at the 200th cycle were 58.6% in the initial electrolyte system and 82.3% in the optimized system.[21] It clearly indicates that the use of HDI helped to raise the capacity of the Cu-TCA. Here the HDI molecules probably preferentially coordinate with the $Cu^{2+}$ ions in the MOF structure. The formed protective layer around Cu ions

might allow screening the negative charge of the oxygen atoms from the $Li^+$ ions and enhancing the structural stability of the Cu-TCA.

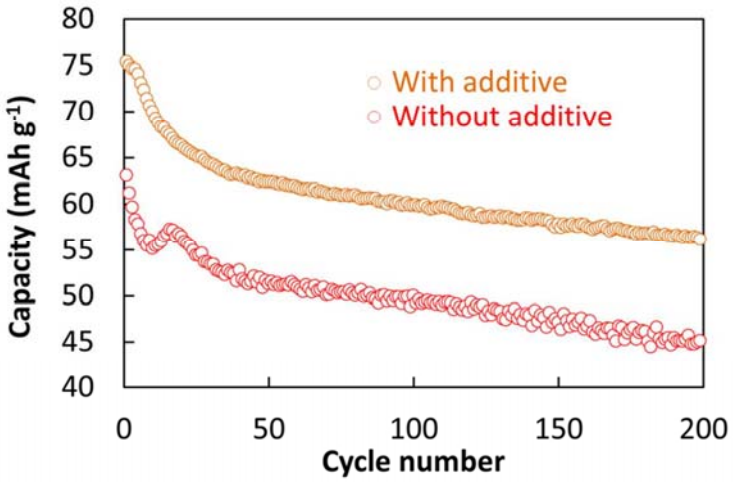


**Figure 6.** Capacity evolutions of the Cu-TCA electrodes for 200 cycles at 2 C rate, with/without the electrolyte additive.

## 4. Conclusion

Using a straightforward method, a MOF material, Cu-TCA ($H_3TCA$ = tricarboxytriphenyl amine) with coexistence of redox active metal and ligand is facilely synthesized. We demonstrated that this MOF material can act as a novel cathode active material for lithium batteries, with comparable high working voltage of 4.3 V to the current commercial $LiCoO_2$ materials. By coupling the electrochemical and physical characterizations, two distinct redox regions were separately identified and attributed to the $Cu^+/Cu^{2+}$ and $N/N^+$ redox couples during charge or discharge process. According to the electrochemical results, we demonstrated that the capacity loss firstly took place around the metal clusters ($Cu^+/Cu^{2+}$), probably due to the restriction of the $Li^+$ ions by carboxylic oxygen atoms leading to the uncompleted redox reactions on the Cu ions and the structural instability of the whole system. Besides, by comparing the performances at recharge rates of 1 C and 2 C, we suggested that the porous

structure of the Cu-TCA materials could be advantageous to sustain their rate capabilities without degrading the capacity retention. Further, by the use of hexamethylene diisocyanate (HDI) as electrolyte addictive, the capacity and the cyclic stability of the Cu-TCA electrode was improved at high capability rate. These investigations could vastly widen the practical application of MOF materials in battery sciences. We believe that this alternative MOF material model could be still improved through rational design of the MOF structure, by introducing other metal clusters (such as $Mn^{2+}/Mn^{4+}$) with higher $Li^{+}$ uptake ability, and by improving the structural resilience of the MOF materials through chemical decorations[22-23].

## ASSOCIATED CONTENT

### Supporting Information

Supplemental charge-discharge curves, TG, SEM and XPS results. This material is available free of charge via the Internet at http://pubs.acs.org.

## AUTHOR INFORMATION

### Corresponding Author

*Zhe Peng, E-mail: pengzhe@nimte.ac.cn

*Xiaohui Yi, E-mail: yixiaohui@nimte.ac.cn

### Notes

The authors declare no competing financial interests.

## ACKNOWLEDGMENT

This work was supported by the 863 project (Grant No. 2013AA050906) and Ningbo Natural Science Foundation (Grant No. 2014A610152). Zhe Peng thanks the financial support from the China Postdoctoral Science Foundation funded project (Grant No. 2015M570530) and Ningbo Natural Science Foundation (Grant No. 2016A610278). Xiaohui Yi thanks the financial support from the China Postdoctoral Science Foundation funded project (Grant No. 2014M560499) and the National Natural Science Foundation of China (Grant No. 61504154).

## REFERENCES

(1) Tarascon, J. M.; Armand, M. Issues and Challenges Facing Rechargeable Lithium Batteries. *Nature* **2001**, 414, 359-367.

(2) Croguennec, L.; Palacin, M. R. Recent Achievements on Inorganic Electrode Materials for Lithium-Ion Batteries. *J. Am. Chem. Soc.* **2015**, 137, 3140-3156.

(3) Denis, S.; Baudrin, E.; Touboul, M.; Tarascon, J. M. Synthesis and Electrochemical Properties of Amorphous Vanadates of General Formula RVO4 (R = In, Cr, Fe, Al, Y) vs. Li. *J. Electrochem. Soc.* **1997**, 144, 4099-4109.

(4) Zhou, H.; Long, J. R.; Yaghi, O. M. Introduction to Metal-Organic Frameworks. *Chem. Rev.* **2012**, 112, 673-674.

(5) Kosaka, W.; Yamagishi, K.; Hori, A.; Sato, H.; Matsuda, R.; Kitagawa, S.; Takata, M.; Miyasaka, H. Selective NO Trapping in the Pores of Chain-Type Complex Assemblies Based on Electronically Activated Paddlewheel-Type [Ru-2(II,II)]/[Rh-2(II,II)] Dimers. *J. Am. Chem. Soc.* **2013**, 135, 18469-18480.

(6) Inokuma, Y.; Yoshioka, S.; Ariyoshi, J.; Arai, T.; Hitora, Y.; Takada, K.; Matsunaga, S.; Rissanen, K.; Fujita, M. X-ray Analysis on the Nanogram to Microgram Scale Using Porous Complexes. *Nature* **2013**, 495, 461-466.

(7) Cho, S.; Ma, B.; Nguyen, S. T.; Hupp, J. T.; Albrecht-Schmitt, T. E. A Metal-organic Framework Material that Functions as An Enantioselective Catalyst for Olefin Epoxidation. *Chem. Commun.* **2006**, 24, 2563-2565.

(8) Férey, G.; Millange, F.; Morcrette, M.; Serre, C.; Doublet, M. L.; Grenèche, J. M.; Tarascon, J. M. Mixed-valence Li/Fe-based Metal-organic Frameworks with Both Reversible Redox and Sorption Properties. *Angew. Chem., Int. Ed.* **2007**, 46, 3259-3263.

(9) Fateeva, A.; Horcajada, P.; Devic, T.; Serre, C.; Marrot, J.; Grenèche, J. M.; Tarascon, J. M.; Maurin, G.; Férey, G. Synthesis, Structure, Characterization, and Redox Properties of the Porous MIL-68(Fe) Solid. *Eur. J. Inorg. Chem.* **2010**, 24, 3789-3794.

(10) Zhang, Z.; Yoshikawa, H.; Awaga, K. Monitoring the Solid-State Electrochemistry of Cu(2,7-AQDC) (AQDC = Anthraquinone Dicarboxylate) in a Lithium Battery: Coexistence of Metal and Ligand Redox Activities in a Metal-Organic Framework. *J. Am. Chem. Soc.* **2014**, 136, 16112-16115.

(11) Suga, T.; Konishi, H.; Nishide, H. Photocrosslinked Nitroxide Polymer Cathode-active Materials for Application in An Organic-based Paper Battery. *Chem. Commun.* **2007**, 17, 1730-1732.

(12) Yoshikawa, H.; Kazama, C.; Awaga, K.; Satoh, M.; Wada, J.; Rechargeable Molecular Cluster Batteries. *Chem. Commun.* **2007**, 30, 3169-3170.

(13) Yoshikawa, H.; Hamanaka, S.; Miyoshi, Y.; Kondo, Y.; Shigematsu, S.; Akutagawa, N.; Sato, M.; Yokoyama, T.; Awaga, K. Rechargeable Batteries Driven by Redox Reactions of Mn12 Clusters with Structural Changes: XAFS Analyses of the Charging/Discharging Processes in Molecular Cluster Batteries. *Inorg. Chem.* **2009**, 48, 9057-9059.

(14) Wang, H.; Hamanaka, S.; Nishimoto, Y.; Irle, S.; Yokoyama, T.; Yoshikawa, H.; Awaga, K. In Operando X-ray Absorption Fine Structure Studies of Polyoxometalate Molecular Cluster Batteries: Polyoxometalates as Electron Sponges. *J. Am. Chem. Soc.* **2012**, 134, 4918-4924.

(15) Wu, P.; Wang, J.; He, C.; Zhang, X.; Wang, Y.; Liu, T.; Duan, C. Luminescent Metal-Organic Frameworks for Selectively Sensing Nitric Oxide in an Aqueous Solution and in Living Cells. *Adv. Funct. Mater.* **2012**, 22, 1698-1703.

(16) Zhang, W.; Wang, C.; Liu, G.; Zhu, X.; Chen, X.; Pan, L.; Tan, H.; Xue, W.; Ji, Z.; Wang, J.; Chen, Y.; Li, R. W. Thermally-stable Resistive Switching with a Large ON/OFF Ratio Achieved in Poly(triphenylamine). *Chem. Commun.* **2014**, 50, 11856-11858.

(17) Beloded, A. A.; Koshechko, V. G.; Pokhodenko, V. D.; Nemoshkalenko, V. V.; Aleshin, V. G. X-ray Photoelectron Spectra of Radical Cations of the Triphenylamine Series and Some Heterocyclic Compounds. *Theor. Exp. Chem.* **1981**, 17, 99-103.

(18) Paschoalinoa, M.; Guedesa, N. C.; Jardima, W.; Mielczarskib, E.; Mielczarskib, J. A.; Bowenc, P.; Kiwid, J. Inactivation of E. coli Mediated by High Surface Area CuO Accelerated by Light Irradiation >360 nm. *J. Photochem. Photobiol., A* **2008**, 199, 105-111.

(19) Wiers, B. M.; Foo, M.-L.; Balsara, N. P.; Long, J. R. A Solid Lithium Electrolyte via Addition of Lithium Isopropoxide to a Metal-Organic Framework with Open Metal Sites. *J. Am. Chem. Soc.* **2011**, 133, 14522-14525.

(20) Wu, F.; Zhu, Q.; Li, L.; Chen, R.; Chen, S. A Diisocyanate/sulfone Binary Electrolyte Based on Lithium Difluoro(oxalate)borate for Lithium Batteries. *J. Mater. Chem. A* **2013**, 1, 3659-3666.

(21) Liu, Y.; Qin, Y.; Peng, Z.; Zhou, J.; Wan, C.; Wang, D. Hexamethylene Diisocyanate as an Electrolyte Additive for High-energy Density Lithium Ion Batteries. *J. Mater. Chem. A* **2015**, 3, 8246-8249.

(22) He, W.; Yuan, D.; Qian, J.; Ai, X.; Yang, H.; Cao, Y. Enhanced High-rate Capability and Cycling Sability of Na-stabilized Layered Li1.2[$Co_{0.13}Ni_{0.13}Mn_{0.54}$]$O_2$ Cathode material. *J. Mater. Chem. A* **2013**, 1, 11397-11403.

(23) Wang, Y. X.; Shang, K. H.; He, W.; Ai, X. P.; Cao, Y. L.; Yang, H. X. Magnesium-Doped $Li_{1.2}[Co_{0.13}Ni_{0.13}Mn_{0.54}]O_2$ for Lithium-Ion Battery Cathode with Enhanced Cycling Stability and Rate Capability. *ACS Appl. Mater. Interfaces* **2015**, 7, 13014-13021.

**Table of Contents Graphic**